Eur. Phys. J. B **51**, 17–23 (2006)
DOI: 10.1140/epjb/e2006-00187-8

THE EUROPEAN PHYSICAL JOURNAL B

Effect of nitrogen concentration on the electronic and vibrational properties of zinc-blende InN_xP_{1-x}($x < 0.01$)

M. Debbichi[1,a], A. Ben Fredj[1], A. Bhouri[1], N. Bouarissa[2], and M. Said[1,b]

[1] Unité de Physique des Solides, Faculté des Sciences de Monastir, Boulevard de l'Environnement, 5019 Monastir, Tunisia
[2] Department of Physics, Faculty of Science, King Khalid University, Abha, P.O. Box 9004, Saudi Arabia

Received 20 August 2005 / Received in final form 6 February 2006
Published online 31 May 2006 –

Abstract. Taking into account the recent advances in the epitaxial growth of single-crystal InN leading to a drastic re-evaluation of its fundamental energy band gap, we have studied the electronic properties of $InN_xP_{1-x}(x < 0.01)$ ternary alloy. Using the empirical pseudopotential method under the virtual crystal approximation, combined with the Harrison bond orbital model, the band gap at Γ, X and L points, the effective masses of the Γ valley and the electronic charge densities are calculated as a function of nitrogen composition. The fitted expressions of the energy band gaps indicate that the bowing parameter at Γ reached a broad value for very low nitrogen incorporation ($x \leq 1\%$). Furthermore, the band gap at Γ point decreases drastically with increasing nitrogen composition up to 1%. The elastic constants and the optical phonon frequencies are also reported. Our theoretical results provide a good agreement with the available data.

PACS. 71.20.Nr Semiconductor compounds – 71.15.-m Methods of electronic structure calculations – 71.15.Dx Computational methodology

1 Introduction

III–V alloys containing nitrogen have undergone rapid development in the past few years. They have been investigated due to their potential applications in long wave length optoelectronic devices [1] and in high efficiency hybrid solar cells [2,3]. Clearly, they offer a new opportunity in a number of technologically important areas. In contrast to conventional alloys in which electronic properties vary smoothly with composition, the incorporation of even a small fraction of nitrogen into the host III–V crystal brings about drastic modification of the electronic properties of the resulting group III-N_x-V_{1-x} alloys. The effect has been observed experimentally in a large variety of III-N-V alloys, such as GaInNAs, GaNP, AlGaNAs and InNP [4–7]. This anomaly is of special interest and has motivated many theoretical efforts to understand the observed results. In fact, different approaches have been proposed. Shan et al. [8] introduced a two-band anticrossing (BAC) model, which predicts a splitting of the conduction band into two subbands with the energy minimum at E_- and E_+. Kent and Zunger [9,10] presented large-supercell calculations, which included effects of the statistical distribution of isolated impurities and various impurity clusters on the band structure. Zhang et al. [11] suggested that the formation of an impurity band which is due to the interaction between different nitrogen-cluster states is responsible for the observed rapid downshift of the conduction-band edge. Bellaïche et al. [12] have found that if the dilute alloys show a localized deep impurity level in the gap, there will be a composition domain in the concentrated alloy where the optical bowing coefficient is large and composition dependent. In the case of $GaP_{1-x}N_x$ alloy, Yaguchi et al. [13] have found that with increasing N concentration, the luminescence peak becomes broader and shift to lower energies. This red-shift behavior is considered to indicate an extremely large band-gap bowing in the $GaP_{1-x}N_x$ alloy system.

Indium phosphide (InP) is a direct-gap semiconductor of great technological significance, since it serves as the substrate for most optoelectronic devices employed in optical communication [14]. However, a low N incorporation into InP will affect the properties of this material [15]. InPN with less than 1%, grown by gas source molecular beam epitaxy (GSMBE), has been studied by Bi and Tu [16]; they found a significant band gap reduction that corresponded to a bowing parameter of about 15 eV [15]. The latter authors attributed the small amount of N incorporation in InP to the very high equilibrium N_2 vapor pressure over InN and the relatively weak In-N bond strength compared to that of InP [16].

Until recently, it was commonly accepted that InN, the narrowest gap number of the nitride family, had a

[a] e-mail: mourad_fsm@yahoo.fr
[b] e-mail: moncef_said@yahoo.fr

Table 1. Pseudopotential form factors and lattice constants for InN and InP.

Compound	Form factors (Ry)						Lattice constant
	$V_s(3)$	$V_s(8)$	$V_s(11)$	$V_A(3)$	$V_A(4)$	$V_A(11)$	a (Å)
InN	–0.330117	0.003930	–0.031435	0.089383	0.320000	–0.006892	4.98[a]
InP	–0.202374	0.000000	0.068796	0.088816	0.060000	0.030000	5.86[a]

[a] Reference [15].

relatively wide gap of 1.9 eV [17]. This gap was determined from optical absorption studies of polycrystalline thin films [17]. Recently, with the use of optical absorption, photoluminescence and photomodulated reflectance experiments, it has been shown that wurtzite InN has a gap in the range 0.7–0.8 eV, which generates significant effects on studies of InN containing group III nitrides alloys. The same value of the energy band gap was recommended for zinc blende InN [18]. This new finding has prompted us to perform calculation of the InN_xP_{1-x} ($x \leq 1\%$) electronic properties using the empirical pseudopotential method (EPM) under the virtual crystal approximation (VCA). Within this model, the alloy is described as a uniform crystal, made of virtual atoms given by a concentration-weighted average of real atoms [19]. In the case of an $A_xB_{1-x}C$ alloy, the virtual atoms replace A and B. This implies that A–C and B–C bonds must be the same, which is not true in general. In the case of InN_xP_{1-x}, the bond length varies substantially from the In-N to the In-P dimmer. As a result of this assumption, it is clear that VCA cannot describe accurately the microscopic atomic environment. However, in spite of its shortcomings, the VCA has been successfully used to model other III–V materials systems [20–25]. Moreover the maximum nitrogen concentration being studied here is 1%. Hence, combining the EPM and the VCA with the Harrison bond-orbital model, we have investigated the electronic, elastic and vibrational properties of InN_xP_{1-x} alloys. To the best of our knowledge, this is the first time such properties have been studied for such an alloy.

In the following we present our results on the band gap energies, the electronic effective masses, the charge density, the elastic constants and the optical phonon frequencies as a function of N content. Our conclusions are summarized in Section 3.

2 Results and discussions

The band-structure calculation is based on the EPM. The form factors for InN and InP are treated as adjustable parameters that are optimized using a non-linear least-squaring procedure [25] and requiring that the calculation reproduces as accurate as possible the observed band gaps at the higher symmetry points in the Brillouin zone. In the case of the zinc blende semiconductor compounds, six pseudopotential form factors, symmetric (V^S) and antisymmetric (V^A), are sufficient to calculate the band structure. For the cubic InN_xP_{1-x} being studied here, the latter parameters are expressed as,

$$V_G^{S,A} = (1-x)V_{\mathrm{InP}}^{S,A} + xV_{\mathrm{InN}}^{S,A}. \quad (1)$$

The lattice constant of the ternary alloy under study is obtained according to Vegard's law,

$$a_{\mathrm{InNP}}(x) = (1-x)a_{\mathrm{InP}} + xa_{\mathrm{InN}}. \quad (2)$$

The final adjusted form factors together with lattice constants for the binary compounds InN and InP are listed in Table 1. In Table 2, we give our energy band gaps, calculated at the principal symmetry points, along with the experimental and theoretical available data in the literature. Generally, there is a reasonable agreement between the available data and our findings.

Table 2. Band gap energies of InP and InN at Γ, X and L high-symmetry points.

Compound	Band-gap energy (eV)		
	E_Γ^Γ	E_Γ^X	E_Γ^L
InN	0.78[a]	2.51[a]	5.82[a]
	0.78[b]	2.51[b]	5.82[b]
	0.7[f]	–	–
InP	1.35[a]	2.38[a]	2.014[a]
	1.423[c]	2.38[c]	2.014[c]
	1.354[d]	–	–
	1.35[e]	2.21[e]	2.05[e]

[a] Present work; [b] reference [17]; [c] reference [15]; [d] reference [43]; [e] reference [44]; [f] reference [45].

2.1 Electronic properties

Figure 1 shows the calculated band-gap energies namely, E_Γ^Γ, E_Γ^X and E_Γ^L as a function of composition x for zinc-blende $InP_{1-x}N_x$. From the results obtained, it is worth noting that only a small N incorporation (x less than 1%) into InP, decreases drastically the fundamental band gap (E_Γ^Γ) of the material of interest. Moreover, E_Γ^X decreases as well with increasing x, while the reverse could be seen for E_Γ^L. Figure 1 shows also $InP_{1-x}N_x$ fundamental band gap as a function of N composition reported from references [16,26] and which are displayed for comparison. In fact, the curve with circles is obtained using the Van Vechten model of the dielectric theory of electro negativity [26] while the triangles referred to experimental results obtained by Bi and Tu [16]. Note that within the

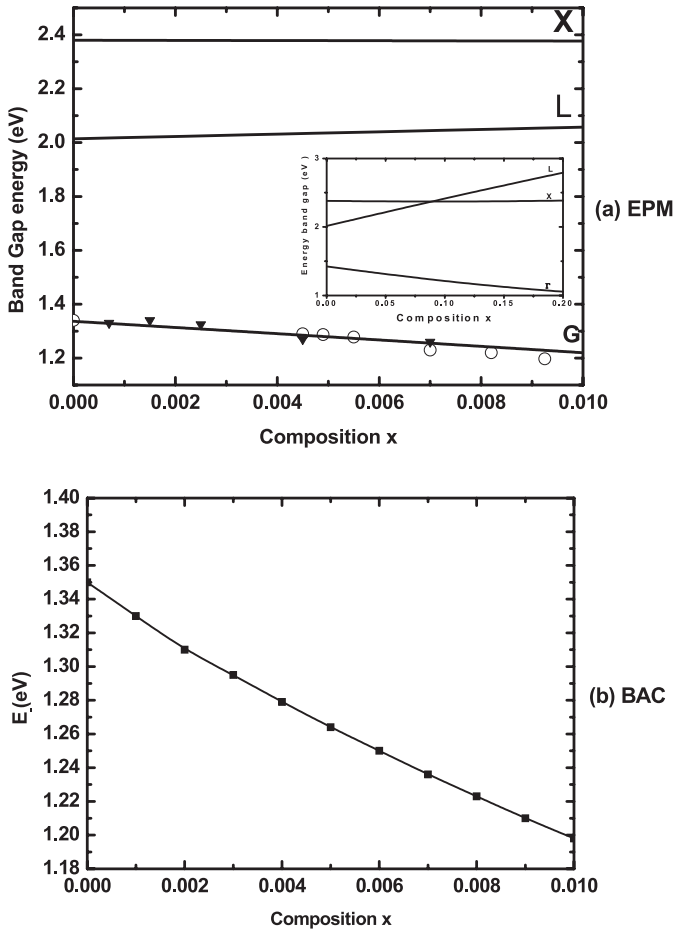

Fig. 1. (a) The nitrogen content- dependent band-gap energies at Γ, X and L points in zinc blende $InP_{1-x}N_x$ (solid curves) in EPM model. Also are shown for comparison, band-gap energy at Γ as reported with the Van Vechten model (circles) and experiment (triangles) [10]. The inset shows the computed E_Γ^Γ, E_Γ^X and E_Γ^L band-gap energies that are for the nitrogen composition range $x = 0$–0.2. (b) The fundamental band gap between the valence band maximum and the E- conduction band minimum as a function of N fraction x of $InP_{1-x}N_x$ in BAC model.

N composition range being studied here ($x \leq 1\%$), our obtained Γ-band gap energy has the same behavior as those reported in references [16,26]. Furthermore, our study of the $InP_{1-x}N_x$ band gap energies at Γ, X and L points for nitrogen composition over the 1%. The inset of Figure 1 shows the computed band gaps which are for the composition range $x = 0$–0.2. The solid lines in the inset of Figure 1 indicate the quadratic least-squares fits to our results. Accordingly, one can point out that a crossover between the L- and X-indirect band gap is found to occur at $x = 0.09$ which corresponds to the band gap energy of 2.37 eV. The composition dependence of $InP_{1-x}N_x$ band gaps over the composition range (0–0.01) can be well fitted by the following quadratic expressions,

$$E_\Gamma^\Gamma(x) = 1.35 - 11.42x + 16.77x^2 \quad (3a)$$

$$E_\Gamma^X(x) = 2.37 - 0.30x + 2.49x^2 \quad (3b)$$

$$E_\Gamma^L(x) = 2.01 + 4.98x - 4.45x^2. \quad (3c)$$

All energies are in electron volts. Note that the optical band-gap bowing behavior, referred by the quadratic terms in equations (3a–3c), occurs differently for the Γ-, X- and L-energy gaps. The L-gap shows a downward bowing but the Γ- and X-gaps show an upward bowing parameters. Moreover, at this region ($x \leq 1\%$), a huge Γ-bowing of 16.77 eV was found, which is more important than X- and L-bowings. The large Γ-band gap bowing is mainly attributed to the localization of the valence charge around nitrogen which in turn is mainly attributed to the large difference in electronegativity between nitrogen and phosphorus. According to Vurgaftman and Meyer [18], the band gap reduction in $InP_{1-x}N_x$ corresponded to a bowing parameter in the range 13–17 eV. The latter authors recommended an average bowing value of 15 eV which agrees reasonably well with our obtained value. In the present study as well as in those of reference [18], the bowing parameter for $InP_{1-x}N_x$ is found composition independent. Leibiger et al. [27] have also obtained a constant bowing parameter $b = 12$ eV for GaN_xP_{1-x} films with $0 \leq x \leq 0.029$. However, a controversy persist on the bowing coefficient for GaAsN: it is independent [28] or dependent [10,12,16] x composition. Based on the BAC model, the fundamental band gap of GaAsN has been calculated by the following equation [18,29]:

$$E_- = \frac{1}{2}\left[\left(E^{\mathrm{N}} + E^C\right) - \sqrt{\left(E^{\mathrm{N}} - E^C\right)^2 + 4V^2 x}\right]$$

where E^C is the energy of the lowest conduction band, E^{N} is the energy of the localized states derived from the substitutional N atoms, V is the term describing the interaction and hybridization between localized N states and the extended states, and x is the N fraction.

Using the parameters mentioned in reference [18], we have recalculated the band gap of dilute GaAsN and deduce a constant bowing $b = 116$ eV. Since GaAs and InP have similar energy gaps and valence-band offsets, it is natural to expect the BAC model to apply equally well to InPN. Using $E^{\mathrm{N}} = 1.79$ eV, $V = 3.0$ eV [18], and $E^C = 1.42$ eV, Figure 2 plots the fundamental band gap as a function of N fraction x for $InP_{1-x}N_x$. It can be seen that in the BAC model the gap decreases about 0.15 eV if x increases 1%, but with the EPM method the gap decreases only 0.11 eV at the same region. With the both models we obtain a constant bowing.

The effective masses are important parameters describing most of carrier transport properties in semiconductor materials such as $InP_{1x}N_x$ alloy. Hence, reliable data of these quantities are needed for the investigation of $InP_{1-x}N_x$ quantum structures. A parabolic line fit to the conduction and valence band dispersions, in the vicinity of the minimum and maximum respectively, is used to determine the electron, heavy-hole (HH) and light-hole (LH) effective masses. Using the standard definition, the density of states electron effective mass can be calculated from the following expression,

$$\frac{1}{m^*} = \frac{4\pi^2}{h^2}\frac{\partial^2 E(k)}{\partial k^2}. \quad (4)$$

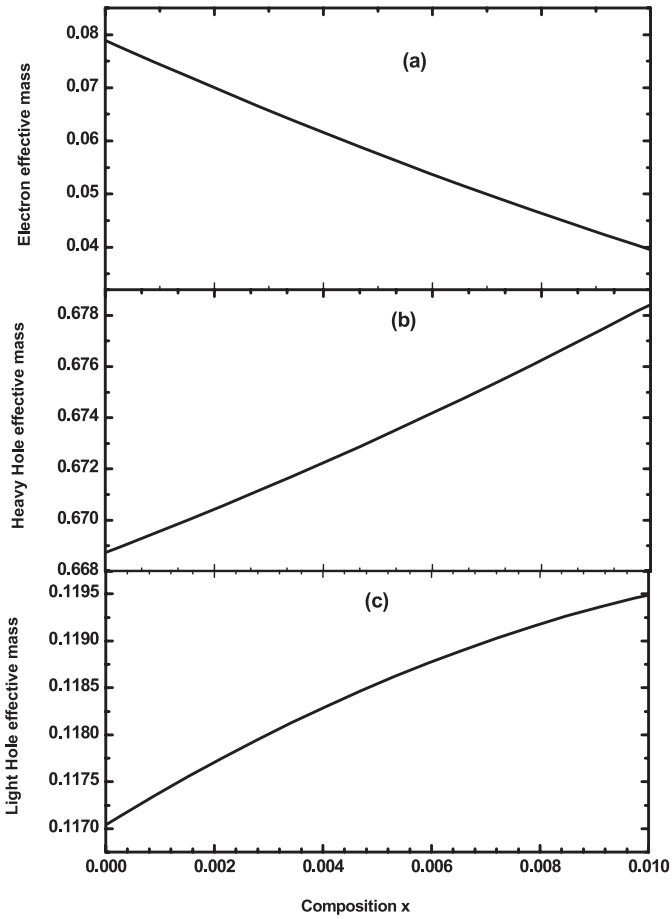

Fig. 2. Effective masses of the (a) electron, (b) heavy hole and (c) light hole (in units of the free electron mass m_0), at the Γ-point of the Brillouin zone in zinc-blende $InP_{1-x}N_x$ as a function of nitrogen content.

Table 3. Conduction and valence band-edge electron, heavy-hole and light-hole effective masses (in units of the free electron mass m_0) at the Γ point of the Brillouin zone in zinc-blende InP and InN.

Effective masses (in units of m_0)			
Material	${m_e}^*$	m^*_{lh}	m^*_{hh}
InN	0.068^a	0.14^a	0.814^a
	0.07 ^{b,c}	0.16^c	0.84^c
InP	0.0789^a	0.117^a	0.668^a
	0.0795^d	0.12^e	0.65^e

[a] Present work; [b] reference [21]; [c] reference [30]; [d] reference [15]; [e] reference [31].

The numerically calculated electron, heavy- and light-hole effective masses for the binary compounds of the material of interest (InPN) are cited in Table 3. In the same table, other theoretical estimates and available experimental values are displayed for comparison. As can be noted, the agreement between the electron effective masses for InN and InP, as derived from our EPM calculations, and the experimental values cited in references [15,21,30] is very satisfactory. For the compound InN, our calculated

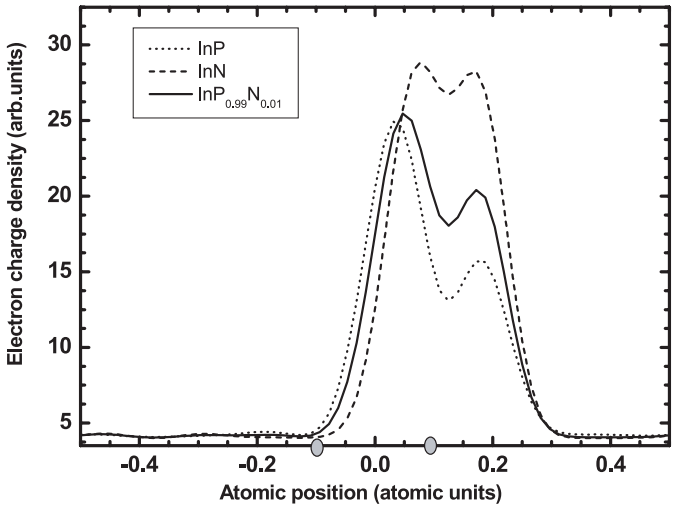

Fig. 3. Total valence charge density at the Γ-point along the [111] direction for zinc-blende InN, InP and $InP_{0.99}N_{0.01}$.

heavy- and light-hole effective masses are closer to those cited in reference [30], whereas in the case of InP, the obtained heavy- and light-hole effective masses agree well with those reported in [31]. The variation of the electron, heavy-hole and light-hole effective masses as a function of nitrogen composition ($x \leq 1\%$) are shown in Figure 2. As can be seen, it is found that: (i) the addition of only a small amount of nitrogen in InP will drastically reduce the electron effective mass of this material. The latter varies from about 0.079 to $0.032m_0$ on going from pure InP to $InP_{1-x}N_x$ with 1% of nitrogen incorporation. Zhang et al. [11] have obtained the same trend: the conduction band effective mass subsequently decreases on further increasing the nitrogen doping, which is precisely what is expected as a result of impurity band formation; (ii) the heavy-hole and light-hole effective masses increase nonlinearly when N content increases from 0 to 1%. The best fit of the calculated effective masses (in units of the free electron mass m_0) has the following forms,

$$m_e(x) = 0.079 - 4.64x + 14.57x^2 \tag{5a}$$

$$m_{hh}(x) = 0.668 + 0.815x + 15.56x^2 \tag{5b}$$

$$m_{lh}(x) = 0.117 + 0.461x - 0.72x^2. \tag{5c}$$

Besides the effective masses, the calculated band structure provides the possibility to determine theoretically the InN_xP_{1-x} electron charge density. The electron charge densities have been found to be a useful probe for understanding chemical bonds in materials [32–34]. The charge density of the nth valence band can be defined as,

$$\rho_n(r) = e \sum_k^{BZ} \Psi^*_{n,k}(r)\Psi_{n,k}(r) \tag{6}$$

here, $\Psi_{n,k}(r)$ are the electronic wave functions. We note that the summation is over all states in the Brillouin zone for a given band n. The total charge density is obtained

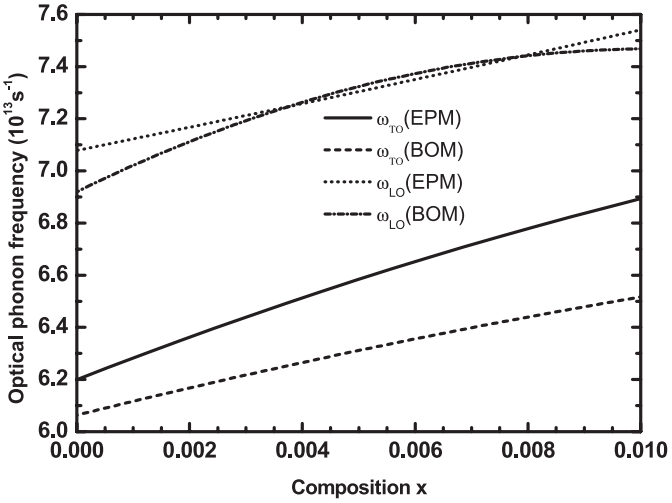

Fig. 4. Optical phonon frequencies in zinc-blende $InP_{1-x}N_x$ ternary alloys as a function of nitrogen content.

Table 4. Elastic constants for zinc-blende $InP_{1-x}N_x$ for different compositions x, compared with other theoretical data.

Material	Elastic constants (GPa)		
	C_{11}	C_{12}	C_{44}
InP	92.1[a]	46.86[a]	42.5[a]
	97[b]	54[b]	45.5[b]
	101[c]	56.2[c]	44.4[c]
$InP_{0.998}N_{0.002}$	95.21	47.02	44.3
$InP_{0.996}N_{0.004}$	97.62	48.2	47.5
$InP_{0.994}N_{0.006}$	100.60	48.8	40.7
$InP_{0.992}N_{0.008}$	104.20	50.0	42.1
$InP_{0.99}N_{0.01}$	109.48	57.4	45.9
InN	246.97[a]	106.6[a]	111.14[a]
	187[d]	125[d]	86[d]
	184[e]	116[e]	177[e]

[a] Present work; [b] reference [46]; [c] reference [47]; [d] reference [15]; [e] reference [37,48].

by adding the charge density from all the occupied valence bands that is:

$$\rho(r) = \sum_n \rho_n(r). \tag{7}$$

In the present work, we are not interested in the total valence charge distribution in the whole Brillouin zone, but only at the high symmetry point Γ ($k = 2\pi/a(0,\,0,\,0)$), a is the lattice constant) in this zone for specific band,

$$\rho(r) = e\,|\Psi_{n,k}(r)|^2\,. \tag{8}$$

In Figure 3, we display the computed electronic charge density along the [111] direction for the sum of the four valence bands at the Γ point for the ternary alloy $InN_{0.01}P_{0.99}$ and its parent compounds InN and InP. The profiles of Figure 3 show that the electronic charge is not equally distributed between the atoms, as being believed for semiconductors with big ionicity. While the topology of the valence density seems to be similar for InN, InP and $InP_{0.99}N_{0.01}$ where the maximum of the charge density of valence electrons that gives the main contribution to the formation of chemical bond is shifted towards the anion and localized in the bonding region. The shift towards the anion seems to become more important as one goes from InP to InN through $InP_{0.99}N_{0.01}$. This could be attributed to the large difference in electronegativity that exists between nitrogen and phosphorus. As a matter of fact, the absence of p electrons in the core of the nitrogen atoms makes the p component of the N pseudopotential rather deep, which favors the transfer of charge towards the nitrogen atoms and results in a larger ionicity than in the rest of the III–V compounds (InP in our case). Practically there is no charge in the interstitial regions both nearest to the anion (N or P) and the cation (In).

2.2 Vibrational properties and elastic constants

The knowledge of mechanical properties and in particular the elastic constants is very interesting to study the effect of strain on electronic properties. Indeed, elastic properties describe the response to an applied macroscopic stress and require knowledge of the curvature of the energy curve as a function of strain for selected deformation of the unit cell. The formulas and procedures for the calculations of the elastic constants used in the present study were described in [35,36].

The numerically calculated elastic constants of $InP_{1-x}N_x$ alloy along with other theoretical results available in the literature are given in Table 4. The agreement between our obtained values and the previously calculated ones for InP is reasonable. Comparison of the calculated InN elastic constants with reported values in the literature is fairly limited, as most of the published data do not use the recent value of InN energy band gap. Since there are no data available in the literature on elastic constants for $InP_{1-x}N_x$ ($0 < x \leq 0.01$) to the best of our knowledge, our calculated values may serve as a reference. The requirement of mechanical stability in cubic crystal leads to the following restrictions on the elastic constants [37], $C_{11} - C_{12} > 0$, $C_{11} > 0$, $C_{44} > 0$ and $C_{11} + 2C_{12} > 0$. Our calculated elastic constants obey this stability criterion for all materials being studied here.

Of particular importance, are the basic vibrational properties, i.e. the longitudinal optical (LO) and transversal optical (TO) phonon frequencies. The LO and TO phonon frequencies have been calculated in the present work for the material of interest using the same procedure used very recently by Bouarissa et al. [38] which consists in combining the Lyddane-Sachs-Teller relation [39],

$$\frac{\omega_{TO}^2}{\omega_{LO}^2} = \frac{\varepsilon_\infty}{\varepsilon_0} \tag{9}$$

with the expression reported in [40],

$$\omega_{LO}^2 - \omega_{TO}^2 = \frac{4\pi\, e_T^{*2} e^2}{M\,\Omega_0 \varepsilon_\infty} \tag{10}$$

Table 5. Transverse effective charge (e_T^*), transversal optical (TO) and longitudinal optical (LO) phonon frequencies of zinc-blende $InP_{1-x}N_x$, for different compositions x.

Composition	e_T^*			$\omega_{TO}(10^{13}$ s$^{-1})$			$\omega_{LO}(10^{13}$ s$^{-1})$		
x	EPM	BOM	Exp	EPM	BOM	Exp	EPM	BOM	Others
0.00	2,41	2.44	2.55[a]	6.20	6.06	5.70[b]	7.06	6.90	6.50[b]
0.002	2.39	2.42	–	6.32	6.18	–	7.20	7.14	–
0.004	2.37	2.40	–	6.55	6.25	–	7.26	7.28	–
0.006	2.35	2.37	–	6.62	6.37	–	7.33	7.36	–
0.008	2.30	2.35	–	6.79	6.43	–	7.44	7.41	–
0.01	2.27	2.31	–	6.89	6.52		7.55	7.49	
InN	2.01	2.07	–	13.4	12.7	–	14.2	13.6	–

[a] Reference [42]; [b] reference [39].

where $\varepsilon_0, \varepsilon_\infty, e_T^*$, M and Ω_0 are the static dielectric constant, the high-frequency dielectric constant, the transverse effective charge, twice the reduced mass and the volume occupied by one atom, respectively. The values of ε_0 and ε_∞ are obtained using the same expressions used in reference [38]. However, for calculating e_T^*, two types of approaches are used. The first approach is based on the pseudopotential [41], while the second one is based on the bond-orbital model (BOM) [35,42]. Within the second model, e_T^* is given by,

$$e_T^* = -\Delta Z + 4\alpha_p + 4\gamma\alpha_p\left(1-\alpha_p^2\right) \tag{11}$$

where α_p is the polarity defined as,

$$\alpha_p = \frac{V_3}{(V_2^2+V_3^2)^{1/2}}. \tag{12}$$

Here, V_2 and V_3 are the hybrid covalent and the hybrid polar energy, respectively. γ is an adjustable parameter with constant value of 0.9 [42], and $\Delta Z = 1$ for III–V compounds.

Our results regarding e_T^*, ω_{TO} and ω_{LO} at various compositions x are listed in Table 5. For comparison, the available experimental data are also reported. A reasonable agreement between our results and the experimental ones could be noticed. The resulting transverse effective charges calculated within EPM are slightly smaller than those obtained using the BOM. The agreement between our results and experiment for e_T^* in InP is better than 6%, whereas for ω_{TO} and ω_{LO} it is better than 9% within EPM and 7% within the BOM. No comparison has been made for $InP_{1-x}N_x$ in the $0 < x \leq 0.01$ composition range, as there are no known data available to date to the best of our knowledge. Figure 4 shows the variation of the frequencies of LO and TO phonons in $InP_{1-x}N_x$ ternary alloys as a function of composition x. Our calculated data are fitted by a least-squares procedure. The analytical expressions are as follows,

(i) EPM approach:

$$\omega_{LO}\left(10^{13}\text{ s}^{-1}\right) = 7.055 + 33.22x - 81.66x^2 \tag{13a}$$

$$\omega_{TO}\left(10^{13}\text{ s}^{-1}\right) = 6.22 + 101.35x - 6.31x^2; \tag{13b}$$

(ii) BOM approach:

$$\omega_{LO}(10^{13}\text{ s}^{-1}) = 6.94 + 120.24x - 38.71x^2 \tag{14a}$$

$$\omega_{TO}(10^{13}\text{ s}^{-1}) = 6.16 + 71.76x - 18.48x^2. \tag{14b}$$

According to Figure 4, as the nitrogen content increases, the LO and TO phonon frequencies increase non-linearly showing generally huge bowing parameters. Qualitatively, almost the same behavior can be noticed within the two methods namely the EPM and BOM. This was not the case for InP_{1-x} Sb_x where it has been reported that increasing Sb content decreases the LO and TO phonon frequencies [38]. Thus, incorporating N into InP instead of Sb leads to the reverse behavior of ω_{TO} and ω_{LO}.

3 Conclusion

In conclusion, a theoretical study of the effect of nitrogen content on the electronic and vibrational properties in zinc-blende $InP_{1-x}N_x$ semiconductor alloys, with a composition x, ranging from 0 to 1% are presented using the empirical pseudopotential method under the virtual crystal approximation, combined with the Harrison bond orbital model. A summary of the key findings follows: (i) $InP_{1-x}N_x$ is a direct band-gap semiconductor within the $0 \leq x \leq 1\%$ composition range; (ii) the fundamental band-gap energy decreases drastically with increasing nitrogen content in the range $0 \leq x \leq 0.01$ making $InP_{1-x}N_x$ suitable for long wave optoelectronic devices; (iii) trends in bonding and ionicity are discussed in the light of the electron valence charge densities at the Γ point for certain N concentrations; (iv) the agreement between our calculated effective masses, elastic constants, and optical phonon frequencies and the available experimental data is very satisfactory. This could be useful for a more understanding of the nitrogen effect on electronic and vibrational properties of nitrogen containing III–V semiconductors. Moreover, our results for non published data may serve as a reference.

M.S. gratefully acknowledges the support of the Abdus Salem-ICTP Trieste, Italy in the framework of the Associateship Scheme.

References

1. M. Kondow, T. Kitatani, S. Naka tsuka, M.C. Larson, K. Nakahara, K. Uomi, H. Inoue, J. Cryst. Crowth **188**, 255 (1998)
2. D.J. Friedman, F.J. Geisz, S.R. Kurtz, D. Myers, J.M. Olson, J. Cryst. Crowth **195**, 409 (1998)
3. S.R. Kurtz, A.A. Allerman, E.D. Jones, J.M. Gee, J.J. Banas, B.E. Hammons, Appl. Phys. Lett. **74**, 729 (1999)
4. M. Weyers, M. Sato, H. Ando, Jpn J. Appl. Phys. **3**, L853 (1992)
5. S. Sakai, Y. Ueta, Y. Teranchi, Jpn J. Appl. Phys. **32**, 4413 (1993)
6. M. Kondow, K. Uomi, K. Hosmi, T. Mozume, Jpn J. Appl. Phys. **33**, L1056 (1994)
7. W. Shan, W. Walukiewicz, K.M. Yu, J. Wu, J.W. Ager III, E.E. Haller, H.P. Xin, C.W. Tu, Appl. Phys. Lett. **76**, 3251 (2000)
8. W. Shan, W. Walukiewicz, J.W. Ager III, Phys. Rev. Lett. **82**, 1221 (1999)
9. P.R.C. Kent, A. Zunger, Phys. Rev. B **64**, 115208 (2001)
10. P.R.C. Kent, A. Zunger, Phys. Rev. Lett. **86**, 2613 (2001)
11. Y. Zhang, A. Mascarenhas, X.P. Xin, C.W. Tu, Phys. Rev. B **61**, 7479 (2000)
12. L. Bellaiche, S.-H. Wei, A. Zunger, Phys. Rev. B **54**, 17568 (1996)
13. H. Yaguchi, S. Miyoshi, G. Biwa, M. Kibune, K. Onabe, Y. Shiraki, R. Ito, J. Cryst. Crowth **170**, 353 (1997)
14. Y.W. Zhao, Z.Y. Dong, M.L. Duan, W.R. Sun, Y.P. Zeng, N.F. Sun, T.N. Sun, Eur. Phys. J. App. Phys. **27**, 167 (2003)
15. I. Vurgaftman, J.R. Meyer, L.R. Ram-Mohan, J. App. Phys. **89**, 5815 (2001)
16. W.G. Bi, C.W. Tu, J. Appl. Phys. **80**, 1934 (1996)
17. J. Wu, W. Walukiewicz, K.M. Yu, J.W. Ager III, E.E. Haller, Hai Lu, W.J. Schaff, Y. Saito, Y. Nanishi, Appl. Phys. Lett. **80**, 3967 (2002)
18. I. Vurgaftman, J.R. Meyer, J. App. Phys. **94**, 3675 (2003)
19. M. Goano, E. Belloti, E. Ghillino, C. Garetto, G. Ghione, K.F. Brennan, J. App. Phys. **88**, 4676 (2000)
20. A. Bhouri, F. Ben Zid, H. Mejri, A. Ben Fredj, N. Bouarissa, M. Said, J. Phys.: Condens. Matt. **14**, 7017 (2002)
21. F. Ben Zid, A. Bhouri, H. Mejri, M. Said, N. Bouarissa, J.-L. Lazzari, F. Arnaud d'Avitaya, J. Derrien, Physica B **322,** 225 (2002)
22. K. Kassali, N. Bouarissa, Microelectronic Engineering **54**, 277 (2000)
23. N. Bouarissa, Phys. Lett. A **245**, 285 (1998)
24. H. Aourag, B. Bouhafs, M. Certier, Phys. Stat. Sol. (b) **201**, 117 (1997)
25. T. Kobayasi, H. Nara, Bull. Coll. Med. Sci. Tohoku Univ. **2**, 7 (1993)
26. K.M. Yu, W. Walukiewicz, J. Wu, J.W. Beeman, J.W. Ager III, E.E. Haller, W. Shan, H.P. Xin, C.W. Tu, Appl. Phys. Lett. **78**, 1077 (2001)
27. G. Leibiger, V. Gottschalch, M. Schubert, G. Benndorf, R. Schwabe, Phys. Rev. B **65**, 245207 (2002)
28. T. Makimoto, H. Saito, T. Nishida, N. Kobayashi, Appl. Phys. Lett. **70**, 2984 (1997)
29. W. Walukiewicz, Physica E **20**, 300 (2004)
30. A. Bhouri, H. Mejri, F. Ben Zid, H. Belmabrouk, M. Said, N. Bouarissa, J.-L. Lazzari, J. Phys.: Condens. Matt. **16**, 511 (2004)
31. K.-H. Hellwege, *LANDOLT-BORNSTEIN Numerical Da to and functional relation ships in science and technology, Group III: Grystal and solid state physics, Semiconductors Subvolume a: physics of group IV element and III–V compounds* (Springer-Verlag, Berlin, 1982) Vol. **17**, pp. 281–97
32. N. Bouarissa, Infrared Phys. Technol. **39**, 265 (1998)
33. N. Bouarissa, Mater. Chem. Phys. **65**, 107 (2000)
34. N. Bouarissa, Eur. Phys. J. B **26**, 153 (2002)
35. J.M. Baranowski, J. Phys. C **17**, 6287 (1984)
36. N. Bouarissa, K. Kassali, Phys. Stat. Sol. (b) **228**, 663 (2001); Erratum 231, 294 (2002)
37. K. Kim, W.R.L. Lambrecht, B. Segall, Phys. Rev. B **53**, 16310 (1996)
38. N. Bouarissa, S. Bougouffa, A. Kamli, Semicond. Sci. Technol. **20**, 265 (2005)
39. C. Kittel, *Introduction to Solid-State Physics*, 5th edn. (New York, Wiley, 1976)
40. S.Y. Davydov, S.K. Tikhonov, Semicondutors **32**, 947 (1998)
41. J.A. Sanjurjo, E. Lopez-Cruz, P. Vogl, M. Cardona, Phys. Rev. B **28**, 4579 (1983)
42. P. Vogl, J. Phys. C **11**, 251 (1978)
43. Detlef Scneider, Detlef Rurup, Bernd Schonfelder, Andreas Schlachetzki, Z. Phys. B **100**, 33 (1996)
44. S. Adachi, J. Appl. Phys. **61**, 4869 (1987) and references cited therein
45. T. Matsuaka, H. Okamoto, M. Nakao, H. Harima, E. Kurimoto, Appl. Phys. Lett. **81**, 1246 (2002)
46. A. de Bernabé, C. Prieto, L. Gonzàlez, Y. Gonzàlez, A.G. Every, J. Phys.: Condens. Matt. **11**, L323 (1999)
47. G. Carlotti, D. Fioretto, L. Polmieri, G. Socino, A. Verdini, C. Rigo, J. Phys.: Condens. Matt. **8**, 2265 (1996)
48. K. Kim, W.R.L. Lambrecht, B. Segall, Phys. Rev. B **50**, 1502 (1994)